



**HAL**  
open science

## Dynamical response of the oceanic eddy field to the North Atlantic Oscillation: a model-data comparison

Thierry Penduff, Bernard Barnier, William K. Dewar, James J. O'Brien

### ► To cite this version:

Thierry Penduff, Bernard Barnier, William K. Dewar, James J. O'Brien. Dynamical response of the oceanic eddy field to the North Atlantic Oscillation: a model-data comparison. *Journal of Physical Oceanography*, 2004, 34 (12), pp.2615-2629. 10.1175/JPO2618.1 . hal-00356729

**HAL Id: hal-00356729**

**<https://hal.science/hal-00356729>**

Submitted on 23 Mar 2020

**HAL** is a multi-disciplinary open access archive for the deposit and dissemination of scientific research documents, whether they are published or not. The documents may come from teaching and research institutions in France or abroad, or from public or private research centers.

L'archive ouverte pluridisciplinaire **HAL**, est destinée au dépôt et à la diffusion de documents scientifiques de niveau recherche, publiés ou non, émanant des établissements d'enseignement et de recherche français ou étrangers, des laboratoires publics ou privés.



Distributed under a Creative Commons Attribution 4.0 International License

# Dynamical Response of the Oceanic Eddy Field to the North Atlantic Oscillation: A Model–Data Comparison

THIERRY PENDUFF\*

*Center for Ocean–Atmospheric Prediction Studies, The Florida State University, Tallahassee, Florida*

BERNARD BARNIER

*Laboratoire des Ecoulements Géophysiques et Industriels, Grenoble, France*

W. K. DEWAR

*Department of Oceanography, The Florida State University, Tallahassee, Florida*

JAMES J. O'BRIEN

*Center for Ocean–Atmospheric Prediction Studies, The Florida State University, Tallahassee, Florida*

## ABSTRACT

Observational studies have shown that in many regions of the World Ocean the eddy kinetic energy (EKE) significantly varies on interannual time scales. Comparing altimeter-derived EKE maps for 1993 and 1996, Stammer and Wunsch have mentioned a significant meridional redistribution of EKE in the North Atlantic Ocean and suggested the possible influence of the North Atlantic Oscillation (NAO) cycle. This hypothesis is examined using 7 yr of Ocean Topography Experiment (TOPEX)/Poseidon altimeter data and three  $1^\circ$ -resolution Atlantic Ocean model simulations performed over the period 1979–2000 during the French “CLIPPER” experiment. The subpolar–subtropical meridional contrast of EKE in the real ocean appears to vary on interannual time scales, and the model reproduces it realistically. The NAO cycle forces the meridional contrast of energy input by the wind. The analysis in this paper suggests that after 1993 the large amplitude of the NAO cycle induces changes in the transport of the baroclinically unstable large-scale circulation (Gulf Stream/North Atlantic Current) and, thus, changes in the EKE distribution. Model results suggest that NAO-like fluctuations were not followed by EKE redistributions before 1994, probably because NAO oscillations were weaker. Strong NAO events after 1994 were followed by gyre-scale EKE fluctuations with a 4–12-month lag, suggesting that complex, nonlinear adjustment processes are involved in this oceanic adjustment.

## 1. Introduction

Altimeter observations are crucial for the study of the ocean variability at different space and time scales. Historically limited to regional and temporary in situ surveys, the monitoring of mesoscale motions has become global and quasi–real time. Sea surface height data provide information about the intensity of the surface eddy activity through the eddy kinetic energy (EKE), that is, the variance of geostrophic surface velocities. Over most of the World Ocean, surface EKE maxima are due

to the instability of the main currents. In a reciprocal way, mesoscale motions affect the path and intensity of the main currents, their interaction with topography (Dewar 1998; de Miranda et al. 1999a), the redistribution and dissipation of potential vorticity (Rhines and Young 1982), convection (Legg et al. 1998), subduction (de Miranda et al. 1999b), transport (e.g., Agulhas rings; Tréguier et al. 2002), and mixing of water masses. The latter processes have time scales comparable to (and are involved in) the oceanic variability at interannual and longer time scales. Stammer et al. (2003, manuscript submitted to *J. Phys. Oceanogr.*) have recently shown that interannual fluctuations of the eddy field intensity, distribution, and subsequent mixing can have important implications for climate simulation. This cause-to-effect relationship is, however, very difficult to explain because it involves the spatially and temporally integrated nonlinear response of the ocean to local and remote

---

\* Current affiliation: Laboratoire des Ecoulements Géophysiques et Industriels, Grenoble, France.

---

*Corresponding author address:* Thierry Penduff, LEGI-MEOM, BP53, 38041 Grenoble Cedex 9, France.  
E-mail: thierry.penduff@hmg.inpg.fr

forcing. To understand the climatic system requires a better description of the interannual variability of mesoscale turbulence in the ocean, its origins, and, ultimately, its effects.

The North Atlantic Ocean is subjected to the North Atlantic Oscillation (NAO), which represents the leading mode of atmospheric variability on interannual to decadal timescales over the basin. This mode modulates the sea level pressure (SLP) difference between Iceland and the Azores from which the NAO index is derived. NAO-related atmospheric fluctuations directly affect the meridional gradient of SLP and thus the location and intensity of the westerlies and its associated storm track (Hurrell 1995; Rogers 1990). Observational, theoretical, and modeling studies show that the response of the North Atlantic large-scale circulation to NAO-related atmospheric variability is complex and largely depends on the time scale considered [see, e.g., the review by Visbeck et al. (2003)].

The oceanic EKE has been shown to follow the seasonal fluctuations of the local wind stress (its intensity, curl, or eddy energy) in certain regions with a few months of lag: 4 months in the eastern North Atlantic (Richardson 1983), 3 months within the Gulf Stream–North Atlantic Current (GS–NAC) system (Garnier and Schopp 1999), and 2 months in the Labrador Sea (White and Heywood 1995). Except in some localized regions, such as the East Greenland Current where the EKE fluctuates in phase with the wind forcing (see White and Heywood 1995), the existence of such a lag led the authors to conclude that the wind drives the seasonal variability of EKE indirectly and/or remotely, that is, through an adjustment of the large-scale flow and/or propagative processes. These processes are complex and have not been clearly identified so far.

Fewer studies have been dedicated to the interannual variability of EKE. A remarkably long (10 yr) current-meter record was collected in the vicinity of the Azores Current (Müller and Siedler 1992), revealing a persistent and strong decrease of EKE during the 1980s. This trend could not be explained unequivocally because of the very local character of the dataset. Based on altimeter data, White and Heywood (1995), Garnier and Schopp (1999), and Ducet and Le Traon (2001) have described the year-to-year evolution of EKE over parts of the North Atlantic. Garnier et al. (2002) have described this variability in the upper South Atlantic from a 5-yr altimeter data-assimilation experiment. An extensive, global-scale description of interannual variability of the surface eddy field was provided by Stammer and Wunsch (1999, noted as SW99 hereinafter) from the 4 yr (1993–96) of Ocean Topography Experiment (TOPEX)/Poseidon altimeter data available at that time. These authors highlighted the significant interannual variability of the eddy field in many regions of the World Ocean and suggested that the EKE decrease detected in the Azores Current area by Müller and Siedler (1992) is due to large-scale adjustment of the ocean circulation to fluctuating forcing

fields. Partly because those studies were based on observations only, the origin of this interannual EKE variability and its possible connection with the atmospheric forcing and/or the large-scale circulation have not been elucidated yet.

An intriguing feature was outlined by SW99 in the North Atlantic. As compared with the 1993 pattern, the 1996 EKE is weaker in subpolar regions and stronger in the subtropics by a considerable amount (20%–30% at gyre scale and up to 70% locally; see their Fig. 1c). This dipolar pattern is basinwide and extends over 10°–20° meridionally. As pointed out by SW99, 1993–96 is actually the period when the winter NAO index became strongly negative. In accord with that fact, the mean westerlies and the associated storm track were both found 10°–20° farther south in 1996 as compared with 1993. The shift of the oceanic turbulence in the North Atlantic might thus be correlated with this atmospheric mode, but SW99 could not demonstrate it because of the short and superficial character of the record. As was shown at seasonal time scale, wind fluctuations may have a strong impact also on the interannual fluctuations of oceanic EKE.

The present study is focused on this North Atlantic dipolar EKE pattern. We perform new diagnostics based (i) on longer TOPEX/Poseidon (T/P) time series and (ii) on the outputs of a 1° numerical model of the Atlantic forced by realistic surface fluxes over the last two decades. The aim of the present study is to provide answers to the following questions.

- 1) Is the model able to simulate (and thus to provide a more detailed description of) the recent EKE evolution diagnosed by SW99?
- 2) If so, has this event been forced by the concomitant NAO transition (as suggested by SW99), and has this connection been robust over the last two decades?
- 3) What does the model–data comparison tell about this interannual variability?

The numerical model and altimeter dataset are presented in sections 2 and 3, respectively. Section 3 describes the processing applied to the model and observed datasets to quantify the interannual variability of the eddy field. The horizontal distribution and temporal evolution of the eddy field in the observed and simulated datasets are presented in section 4. The link between the large-scale distribution of the eddy field and the NAO index is discussed in section 5, and conclusions are given in section 6.

## 2. Model configuration and experiments

The numerical data used in this study were produced during the “CLIPPER” experiment (Tréguier et al. 1999). The model used is Océan Parallélisé, version 8.1 (usually referred to as OPA 8.1; Madec et al. 1988), a geopotential-coordinate primitive equation model with

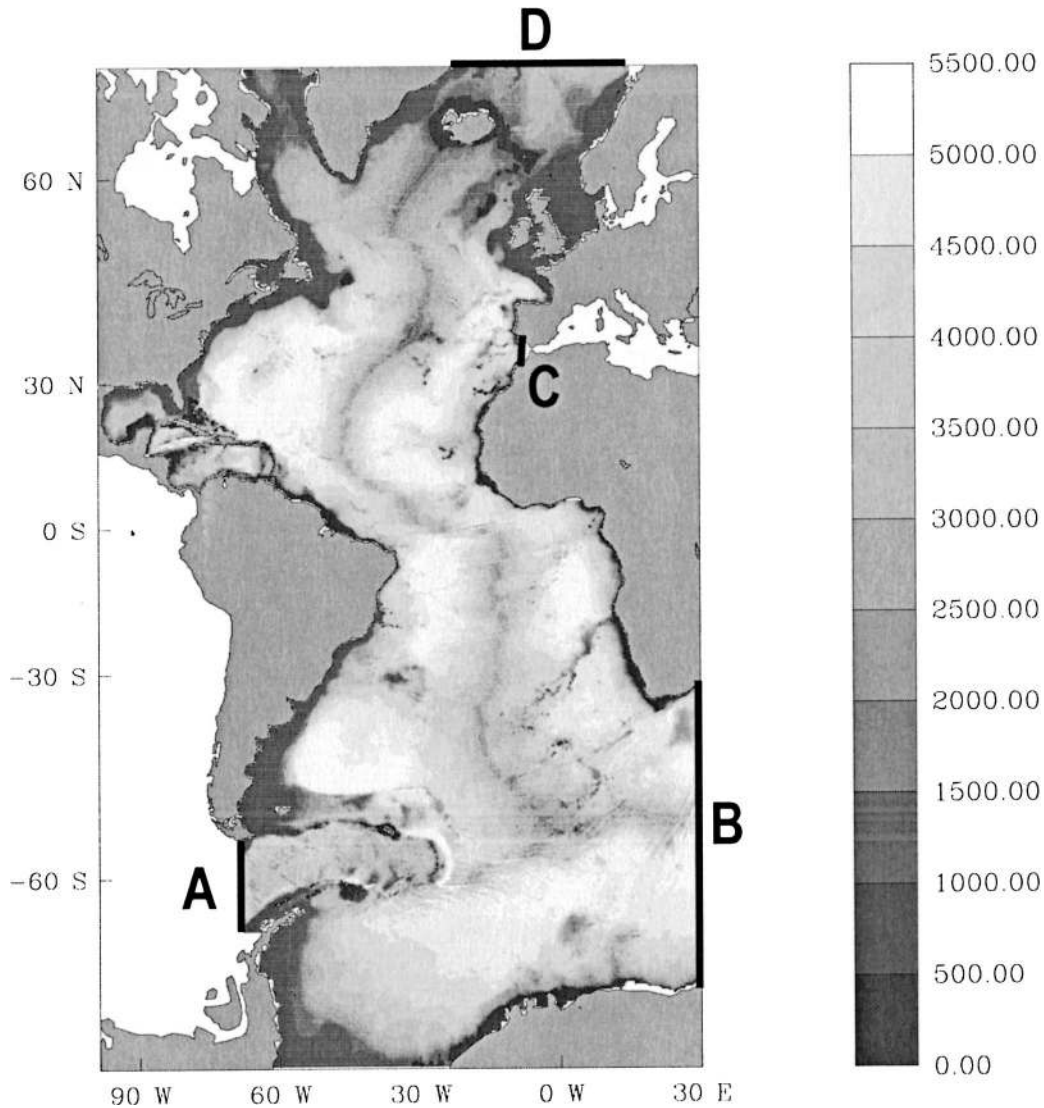


FIG. 1. Model bathymetry (m) and domain. Black lines locate the four open boundaries.

rigid lid implemented on a  $1^\circ$  Mercator grid on the whole Atlantic with 42 levels in the vertical direction. The vertical grid spacing increases from 12 m at the surface to 250 m below 1500 m. Horizontal diffusion and viscosity are parameterized as biharmonic operators. The vertical mixing coefficient is given by a second-order closure scheme (Blanke and Delecluse 1993) and is enhanced in case of static instability. The bottom topography (Fig. 1) is based on the Smith and Sandwell (1997) database. The domain is limited by four open boundaries located at  $70^\circ\text{N}$ , in the Gulf of Cadiz ( $8^\circ\text{W}$ ), at the Drake Passage ( $68^\circ\text{W}$ ), and between Africa and Antarctica ( $30^\circ\text{E}$ ). These Orlanski-type open boundaries radiate perturbations outward and relax the model variables to a climatological reference. Details about the implementation and behavior of the open boundaries are given in Tréguier et al. (2001). Model outputs are saved

as successive 5-day averages to avoid the aliasing of high-frequency processes (Crosnier et al. 2001).

The model is started from rest with temperature and salinity fields taken from the Reynaud et al. (1998) climatological analysis and then is spun up for 8 yr with a climatological, low-passed (cutoff period at 10 days), daily seasonal forcing computed from the 1979–93 European Centre for Medium-Range Weather Forecasts (ECMWF) ERA15 reanalysis. Despite its relatively short duration, this spinup is long enough to stabilize the location of major fronts. In the experiment labeled HF (high frequency), the model is forced from the end of the spinup by the daily ECMWF reanalysis between 1979 and the end of 1993 and by ECMWF analyses between 1994 and 2000 (both interpolated at every time step). Wind stress time series at each latitude did not exhibit any noticeable discontinuity on 1 January 1994.

TABLE 1. Model integrations.

Integration	Forcing	Initial state	Integration period
Spinup	Climatological seasonal cycle deduced from ERA-15 ECMWF reanalysis	Reynaud et al. (1998) climatological data, state of rest	8 yr
HF (high frequency)	Daily ECMWF reanalysis (1979–93) and analysis (1994–2000)	End of spinup (14 Feb 1979)	1979–2000
LF (low frequency)	Low-passed HF forcing (cutoff period: 1 month)	HF state on 21 Mar 1992	21 Mar 1992 until 31 Dec 1999
PF (periodic forcing)	Same as spinup	End of spinup (1979)	Spinup forcing repeated until 31 Dec 1999

Reanalyzed and analyzed wind stress datasets were thus linked to each other without modification. On the contrary, time-averaged heat and salt fluxes did exhibit a jump between the reanalysis and analysis periods. Continuity was insured by replacing their 1994–2000 temporal means by their 1980–93 counterparts from the reanalysis. As shown hereinafter, this treatment does not affect our study, which is focused on intradecadal time scales. A second integration labeled LF (low frequency) was started from the HF state on 21 March 1992 until the end of 1999. A low-pass Lanczos filter with a 35-day cutoff period was applied to the HF surface forcing (wind stress, heat, and salinity fluxes) to generate LF forcing fields in which temporal variability at scales shorter than 1 month were filtered out. A third simulation, labeled PF (periodic forcing) is a continuation of the spinup: it was forced between 1979 and the end of 2000 (arbitrary years) by the same climatological seasonal cycle to provide complementary information about the interannual variability generated intrinsically. Table 1 summarizes the three model integrations.

The wind stress is applied as a boundary condition in the momentum equations in the three runs. Heat and virtual salinity fluxes are imposed as described in Barnier (1998): ECMWF fluxes are introduced as source terms in the temperature and salinity equations at the uppermost level and are corrected by a retroaction term. This term is proportional to the difference between the tracer value in the model [sea-surface temperature (SST) or salinity (SSS)] and an observed value: weekly SST from Reynolds and Smith (1995) and seasonal climatological SSS from Reynaud et al. (1998). The proportionality coefficient depends on time and space as explained in Barnier (1998).

### 3. TOPEX/Poseidon data, definition of EKE, and processing

We made use of sea level anomaly (SLA) maps deduced from TOPEX/Poseidon altimeter time series, available every 10 days between 22 October 1992 and 29 December 2000 at a resolution of  $0.25^\circ$  by  $0.25^\circ$ . These fields were built using an improved space/time objective-analysis method that takes into account long-wavelength errors and correlated noise (Le Traon et al. 1998). Because SLAs are not directly simulated by our

rigid-lid model, we will compare the simulated and observed eddy activities from near-surface geostrophic velocities, which derive from SLA data at time  $it$  as

$$\begin{pmatrix} u_{it} \\ v_{it} \end{pmatrix} = \frac{g}{f} \mathbf{k} \times \nabla(\text{SLA}_{it}).$$

Model velocities are considered at 55 m, that is, below the ageostrophic Ekman layer. To be precise, we compare the variances of these two velocity fields, that is, the observed and simulated eddy kinetic energies. EKE time series (noted  $\text{EKE}^\circ$  hereinafter) are often (e.g., SW99; Garnier and Schopp 1999) derived from geostrophic velocity time series  $(u_{it}, v_{it})$ ,  $it \in [1, Nt]$  as follows:

$$\text{EKE}_{it}^\circ = [(u_{it} - \bar{u})^2 + (v_{it} - \bar{v})^2]/2,$$

where  $it$  is the time stepping index, and  $Nt$  is the total number of records in the time series. Time averages are computed over the whole time series as

$$\begin{pmatrix} \bar{u} \\ \bar{v} \end{pmatrix} = \frac{1}{Nt} \sum_{it=1}^{Nt} \begin{pmatrix} u_{it} \\ v_{it} \end{pmatrix}.$$

The resulting  $\text{EKE}^\circ$  time series quantifies the fluctuations of the kinetic energy. However, all time scales resolved in the dataset contribute to  $\text{EKE}^\circ$ —that is, not only those associated with mesoscale turbulence (in which most authors are interested), but also those with interannual velocity fluctuations. The latter should not be assumed as small a priori. In the North Atlantic for example, the number, location, and transport of the branches of the North Atlantic Current are highly variable (Sy et al. 1992; White and Heywood 1995). The location and intensity of the Azores Current are also subject to interannual variability (Klein and Siedler 1989). The contribution of interannual velocity fluctuations can be removed from EKE estimates while keeping the mesoscale contribution by computing successive annual EKEs (velocity variances over 1 yr). This is the choice made by SW99, but it would provide only seven EKE estimates over our 7-yr T/P time series: the high temporal resolution provided by  $\text{EKE}^\circ$  is lost.

We thus computed EKE time series (denoted  $\text{EKE}_{it}^y$ , where the subscript  $y$  means “year”) as running variances of the velocity field over overlapping 1-yr time intervals at time  $it$ :

$$\text{EKE}_{it}^y = [(u_{it} - \bar{u}_{it}^y)^2 + (v_{it} - \bar{v}_{it}^y)^2]/2,$$

where

$$\begin{pmatrix} \bar{u}_{it}^y \\ \bar{v}_{it}^y \end{pmatrix} = \frac{1}{1 \text{ year}} \sum_{i=it-6 \text{ months}}^{it+6 \text{ months}} \begin{pmatrix} u_i \\ v_i \end{pmatrix}$$

is the running mean of velocities. The above quantities were computed every 5 days from the model outputs and every 10 days from T/P data, excluding the first and last 6 months. The  $\text{EKE}^y$  time series fits our requirements because it captures the intensity of velocity fluctuations on time scales shorter than 1 yr at high temporal resolution. However, the seasonal cycle of the velocity field is not monochromatic and has time scales that overlap those of mesoscale turbulence. Both processes are thus impossible to separate properly, even by defining running variances over 6-month windows (as we did in a preliminary sensitivity study) or by subtracting a mean seasonal cycle from the velocity time series before variance computations. The seasonal cycle of velocity is thus merged with the mesoscale signal in each  $\text{EKE}_{it}^y$  and does not appear in the resulting time series. This formulation is adequate because we are interested in the interannual variability of EKE. EKE will refer to  $\text{EKE}^y$  in the following, unless stated otherwise.

Local EKEs have been computed also from a  $1^\circ$ -resolution CLIPPER simulation initialized and forced exactly as the HF simulation. This coarse-resolution EKE quantifies the variance of seasonally varying velocity fluctuations without any turbulent contribution and turns out to be 1/15–1/40 of that in the  $1^\circ$  run. Moreover, there is no phase link between the EKE fluctuations diagnosed from both runs, showing that mesoscale turbulence is largely responsible for the features described in the present paper.

To summarize, 10-day/0.25°-resolution T/P SLA maps were treated as follows: Computation of anomalous geostrophic velocities  $u'$  from SLA maps, bilinear interpolation of  $u'$  on the isotropic model grid ( $1^\circ$  resolution) and computation of  $\text{EKE}_{\text{TP}}$ , the running variance of velocities over 1-yr windows every 10 days between 30 April 1993 (6 months after the first available SLA map) and 4 January 2000. Model velocities were taken every 5 days at 55-m depth to compute  $\text{EKE}_{\text{model}}$  (exactly like  $\text{EKE}_{\text{TP}}$ ) between 7 July 1980 and 3 July 1999.  $\text{EKE}_{\text{model}}$  was also estimated from the same velocity time series subsampled at a 10-day period (like T/P data), but the difference with its 5-day version was not noticeable. Space- and time-dependent  $\text{EKE}_{\text{TP}}$  and  $\text{EKE}_{\text{model}}$  fields were eventually averaged temporally to produce mean EKE fields or horizontally to estimate the gyre-scale EKE variability. The horizontal structure and temporal fluctuations of these running variances are discussed below.

## 4. Time average and gyre-scale variability of EKE

In this section we address the first question raised in the introduction by comparing the spatial and temporal structures of the observed and simulated EKE fields.

### a. Observed and modeled mean EKE fields

The overall distribution and averaged level of mean EKE from the HF simulation is in reasonable agreement with observed data (Fig. 2). The most energetic regions are found within the North Equatorial Countercurrent retroflection region (very realistic model EKE level), within the Caribbean Sea (overestimated EKE), within the Azores Current (local maximum of EKE well located but underestimated), and within the GS–NAC. Along this latter current system, model EKE reaches a maximum just downstream of Cape Hatteras instead of the elongated EKE band observed between  $70^\circ$  and  $50^\circ\text{W}$ . As in most geopotential-coordinate model simulations (even at the present resolution), this EKE maximum is associated with an unrealistic overshoot of the Gulf Stream and a pulsating standing eddy located at the Gulf Stream separation point. The NAC path and associated EKE field also exhibit some discrepancies in the central basin. Instead of flowing north and creating an EKE maximum between  $50^\circ$  and  $40^\circ\text{W}$  as observed, the simulated NAC and associated EKE maximum extend northeastward across the Mid-Atlantic Ridge, leading to an overestimated EKE in the eastern basin. However, as shown later, this mean bias does not adversely affect the EKE variability studied here.

### b. Meridional redistribution of EKE between 1993 and 1996

Figure 3a shows the relative change  $R = C/M$  of yearly EKE between 1993 and 1996 from T/P data, that is, its absolute change  $C$  divided by its temporal mean  $M$ . As expected from our similar data processing techniques, this figure does not differ much from SW99's Fig. 1c and shows that EKE has substantially decreased (increased) north (south) of about  $45^\circ\text{N}$  over this period. This change was proven statistically significant by SW99. Relative change  $R$  was computed from the HF simulation (Fig. 3b) as  $R = C/(M + E)$ , where  $E$  corresponds to the mean EKE model bias in the eastern subtropical gyre ( $E = 15 \text{ cm}^2 \text{ s}^{-2}$ ). This correction avoids a spurious overestimation of  $R$  in quiet regions by bringing simulated  $M + E$  levels close to observed  $M$  values. Figure 3a shows that, despite local differences, the model does reproduce fairly well the gyre-scale dipolar EKE pattern mentioned by SW99. This conclusion answers the first question raised in the introduction.

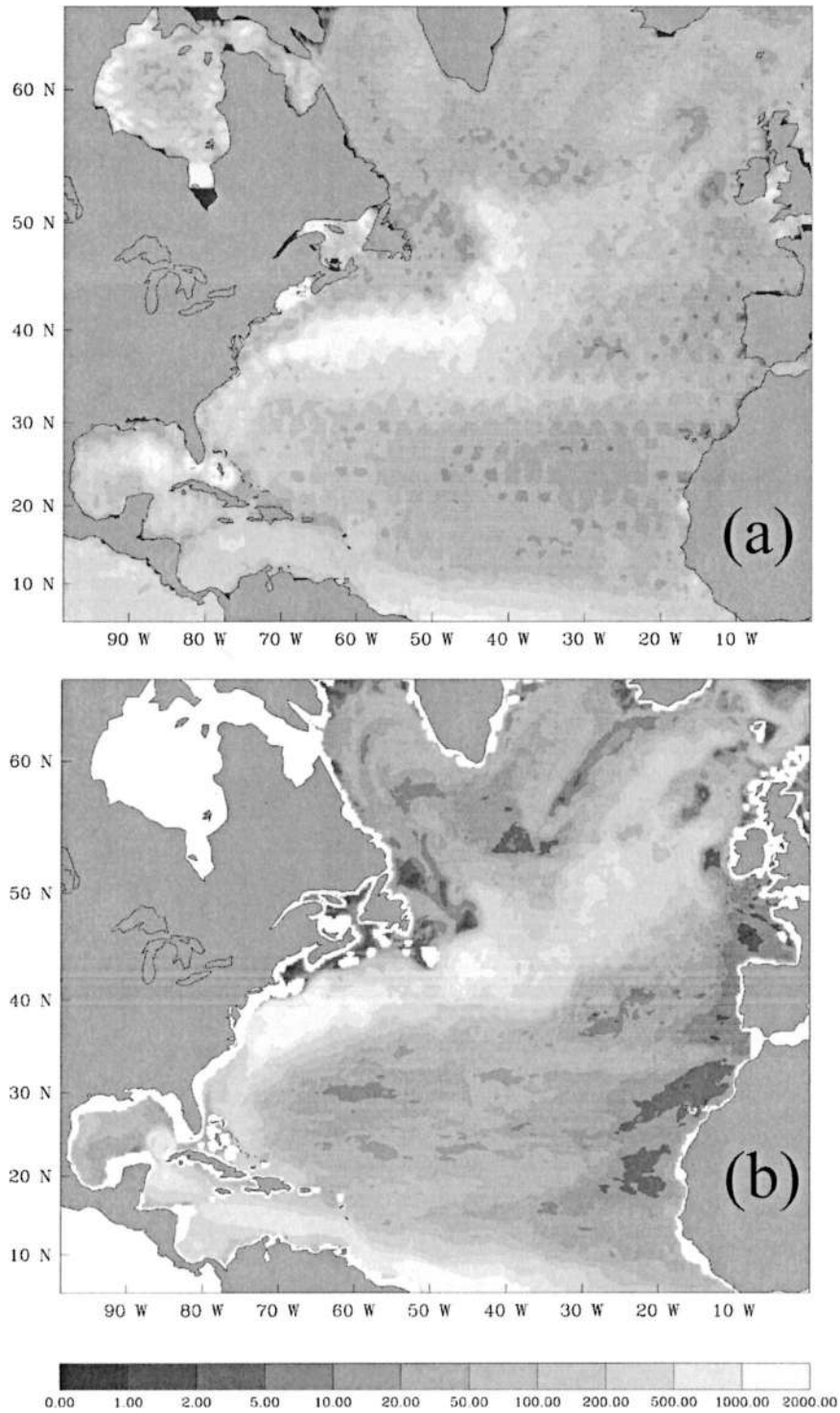


FIG. 2. Averages of yearly eddy kinetic energies (EKE;  $\text{cm}^2 \text{s}^{-2}$ ) for the period 1993–2000 from (a) TOPEX/Poseidon data and (b) the HF simulation at 55 m. Maxima in shallow regions [(a)] mostly reflect tidal errors and should not be taken into account when comparing both panels. These EKEs are computed over individual years (running EKEs on 1 Jul) and are averaged over these years. The grayscale is the same for both (a) and (b).

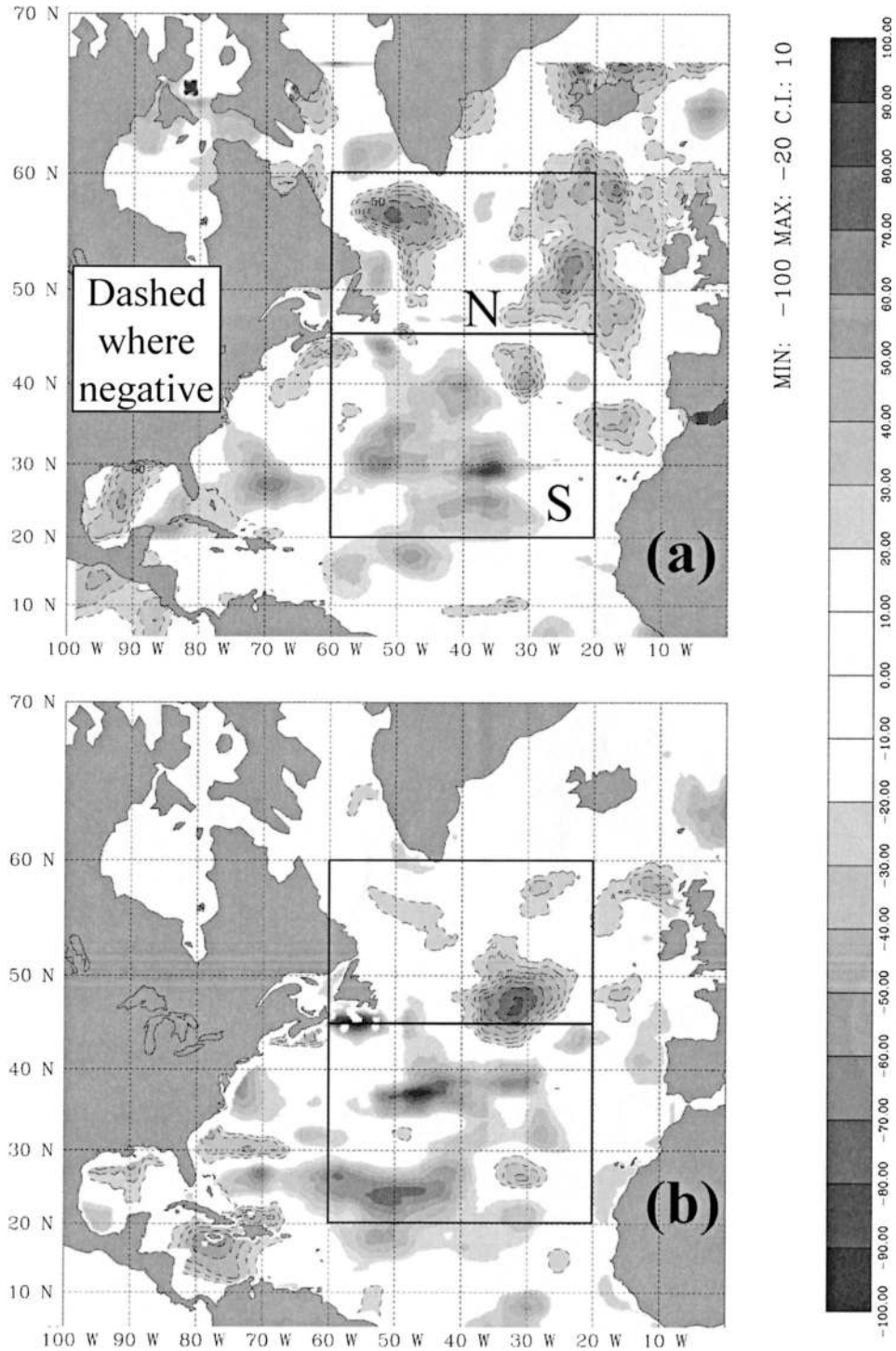


FIG. 3. Difference of EKE between 1996 and 1993 normalized by the averaged EKEs between 1993 and 1996:  $100\% \times (EKE_{1996} - EKE_{1993}) / [(EKE_{1993} + EKE_{1994} + EKE_{1995} + EKE_{1996})/4 + E]$  (see text about the constant value  $E$ ). The resulting quantity was smoothed to highlight large-scale structures. Dashed contours indicate negative values. (a) TOPEX/Poseidon data with  $E = 0$ , and (b) HF simulation outputs with  $E = 15 \text{ cm}^2 \text{ s}^{-2}$ . Rectangles represent the northern and southern boxes over which EKE is computed and displayed in Fig. 4.

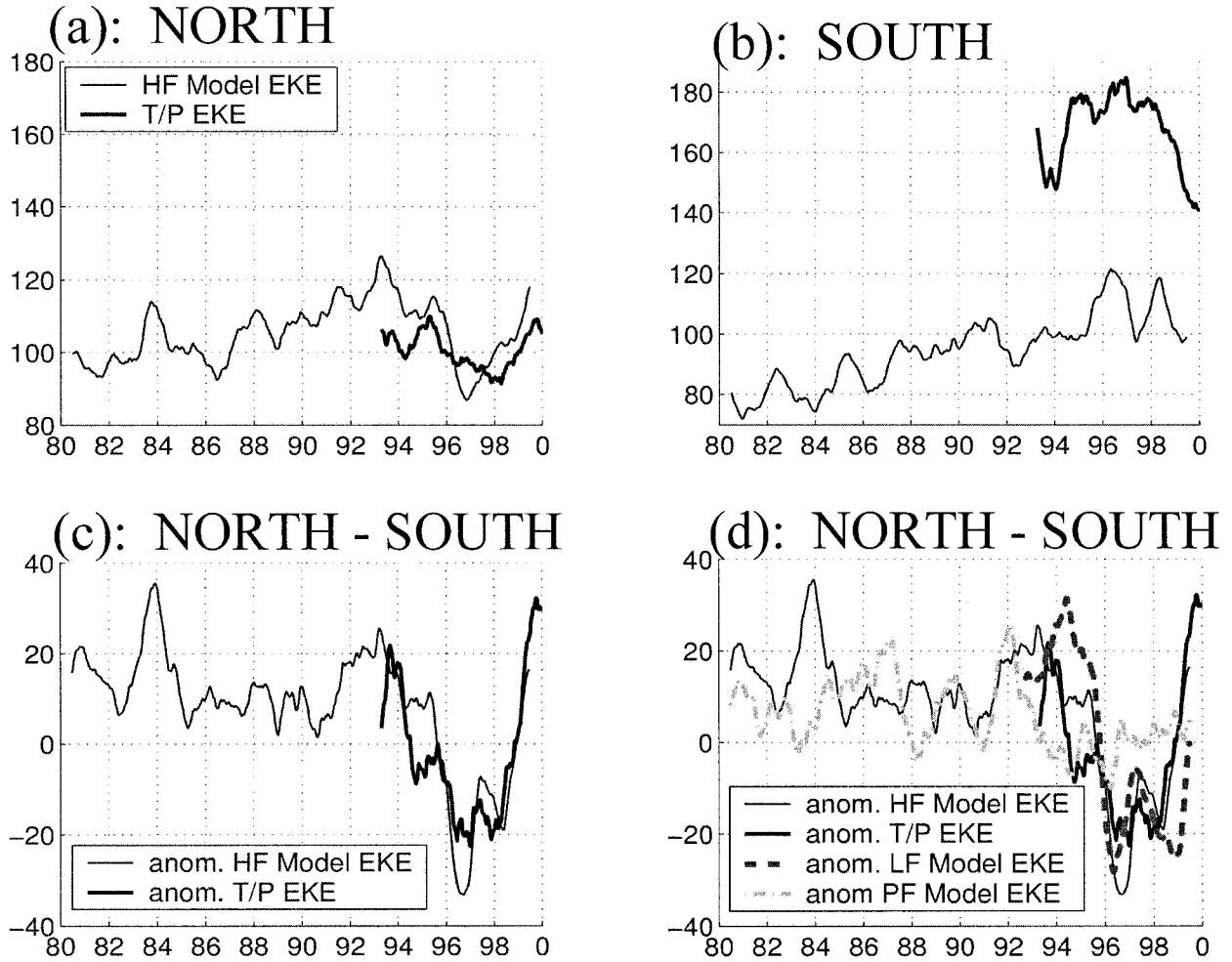


FIG. 4. Temporal evolution of T/P and HF simulation EKE ( $\text{cm}^2 \text{s}^{-2}$ ), horizontally averaged in the (a) southern box and (b) northern box shown in Fig. 3. (c) Anomaly of the EKE meridional contrast ( $\text{EKE}_{\text{north}} - \text{EKE}_{\text{south}}$ ;  $\text{cm}^2 \text{s}^{-2}$ ) from T/P and from the HF model simulation. (d) Same as (c) with EKE contrasts diagnosed from simulations LF and PF. Differences in (c) and (d) are presented in anomaly with respect to their mean over 1993–99.

### c. Temporal evolution of subpolar and subtropical EKE

Running EKEs obtained from model simulations and deduced from T/P data were averaged within the two boxes shown in Fig. 3a. Results are presented in Fig. 4. In the following discussion, the meridional contrast of a variable refers to the difference between its subpolar and subtropical spatial averages.

In the northern box (Fig. 4a),  $\text{EKE}_{\text{TP}}$  fluctuates around  $100 \text{ cm}^2 \text{ s}^{-2}$ . It decreases during 1993, increases until mid-1995, decreases until early 1998, and finally increases until late 1999.  $\text{EKE}_{\text{HF}}$  exhibits a positive trend (close to  $1.7 \text{ cm}^2 \text{ s}^{-2} \text{ yr}^{-1}$ ) that is also visible in the southern box (Fig. 4b). These trends thus cancel in the meridional EKE contrast. The magnitude of subpolar EKE and its overall temporal evolution (especially the marked EKE minimum observed between 1996 and 1998) are realistically simulated over this 7-yr period with the HF forcing with the exception of the 1995–96

period when the decrease of simulated subpolar EKE is not confirmed by altimeter data.

In the southern box (Fig. 4b),  $\text{EKE}_{\text{TP}}$  increases between 1994 and 1996 and decreases between 1998 and 2000 with two or three oscillations at a time scale of about 2 yr.  $\text{EKE}_{\text{HF}}$  in this box is weaker than  $\text{EKE}_{\text{TP}}$  by about 30% with a positive trend (commented below); it increases in 1995—that is, 1 yr after observed—and then exhibits the same kind of 2-yr modulation approximately in phase with observations. In accordance with T/P data, the model produces the highest subtropical EKE values between 1995 and 1998.

Observations show that the mean level of EKE is stronger in the subtropical box than in the subpolar box, whereas both levels are of the same order in the HF simulation. Figure 2 shows that this comes from an overestimation of  $\text{EKE}_{\text{HF}}$  in the eastern part of the North Atlantic Current and, probably to a lesser extent, an underestimation of  $\text{EKE}_{\text{HF}}$  in the Azores Current (south-

ern box). Despite these differences in mean EKE, the interannual variability of EKE turns out to be simulated well in both regions and comparable to observations over the T/P mission.

#### *d. Temporal evolution of the EKE meridional contrast*

A negative meridional  $EKE_{TP}$  contrast anomaly builds up between 1993 and 1995 (thick line in Fig. 4c), reaches about  $-40 \text{ cm}^2 \text{ s}^{-2}$ , and vanishes between 1998 and 1999. Superimposed over this 7-yr evolution, a modulation is clearly visible at a shorter period (1.5–2 yr) between 1993 and the end of 1997.  $EKE_{HF}$  and  $EKE_{TP}$  contrasts are remarkably similar: their mutual correlation is 0.83 (unsmoothed time series). The linear trends already mentioned in both subpolar and subtropical simulated EKEs correspond to an intrinsic long-term adjustment of the model energy since they are also present in the PF simulation.

According to the HF simulation (Fig. 3a), the strongest change in EKE contrast occurred during the T/P mission, when the northern and southern EKEs anomalies were out of phase. The 1993–96 decrease is sampled well from the dataset that was available to SW99. Another strong change in  $EKE_{HF}$  contrast occurred in 1982–85, but the realism of this event cannot be confirmed from observations because our altimeter dataset starts in 1993.

### **5. Discussion: Link between the NAO and the meridional contrast of EKE**

SW99 have mentioned that both the westerlies and the storm track shifted southward between 1993 and 1996 in the North Atlantic (their Fig. 14), in accordance with the evolution of the NAO index. They suggest the existence of a link between the NAO cycle and the EKE contrast through the energy input by the wind into the ocean. We computed the meridional contrast of the energy input by the wind stress  $\tau$  as the difference of  $(\mathbf{u} \cdot \tau)$  averaged over the subpolar and the subtropical gyres ( $\mathbf{u}$  denotes the model surface velocities). This contrast (Fig. 5a) exhibits a strong monthly variability and seems to follow the NAO index with no lag. Indeed, there is a clear zero-lagged correlation between these monthly time series over the 20 yr of integration (Fig. 5d). We now address the last two questions raised in the introduction.

#### *a. Lag between the NAO and the EKE contrast*

The cross correlation between the unfiltered time series of NAO index and EKE contrast (shown in Fig. 5a) will be referred to as  $C(\text{lag})$  in the following. It was computed over the three thirds of the HF integration because only an intermittent connection between the NAO and the EKE contrast is expected. The plain lines

in Fig. 5c show  $C(\text{lag})$  for the three thirds of the HF integration. The black lines in Figs. 5e and 5f are identical to the green line in Fig. 5c. The  $C(\text{lag})$  was also computed from  $EKE_{TP}$  time series over the last period (result shown as a thick black line in Fig. 5f).

This latter panel confirms that the  $EKE_{TP}$  contrast follows the NAO cycle with few months of lag after 1994 (relatively high  $C$  between 0 and 12 months, maximum around 5 months, and secondary maximum at 10 months). A connection between NAO and  $EKE_{HF}$  appears after 1994, as expected from Fig. 5b:  $C(\text{lag})$  in the HF run is close to the observed one over the lag range 0–6 months, reaches its maximum around 10 months (in accordance with the secondary maximum derived from observations), and drops at higher lags. No connection between NAO and  $EKE_{HF}$  is found over the first two-thirds of the integration [ $C(\text{lag})$  is much smaller in Fig. 5c]. The significance of these cross correlations and the presence of high  $C(\text{lag})$  values in HF within the band 8–12 months are discussed in the following sections.

#### *b. Significance of correlations*

The significance of  $C(\text{lag})$  in the HF run may be estimated from its counterparts in the PF run (dashed lines in Fig. 5c) in which no NAO forcing is applied and thus no significant  $C(\text{lag})$  is expected. The hypothesis of an NAO–EKE connection between 1994 and 1999 in the HF run is supported by three facts. 1) Cross correlation  $C(\text{lag})$  is significant in the HF run over the period 1994–99; indeed, the green line in Fig. 5c is located above the dashed lines. 2) The high correlation (0.83) found after 1994 between T/P and HF EKE contrast monthly time series falls to zero ( $-0.07$ ) in the PF run. 3) In 1996, the  $EKE_{HF}$  contrast anomaly (plain thin line in Fig. 4d) exceeds 4.5 times the standard deviation of  $EKE_{PF}$  ( $\sigma_{PF} = 7.4 \text{ cm}^2 \text{ s}^{-2}$ , dot-dashed gray line). The evolution of  $EKE_{HF}$  contrast over the period of 1994–99 was thus certainly forced by the interannual atmospheric forcing (i.e., by the NAO cycle that dominates it) with a few months of lag. In contrast, the  $EKE_{HF}$  contrast in 1982–85 is not significantly correlated with the NAO (plain black line in Fig. 5c), despite the resemblance and phase relationship between the corresponding blue and red peaks in Fig. 5b. We shall thus focus on the 1994–99 period in the following. We did not directly estimate the significance of  $C(\text{lag})$  deduced from T/P data, but the observed EKE anomaly between 1993 and 1996 (Fig. 3a) was proven significant by SW99; it reaches  $3\sigma_{PF}$  in 1996.

SW99’s hypothesis is thus supported very well by our results. The NAO index fluctuations affect 1) the meridional contrast of energy transferred by the wind to the ocean with no significant lag and 2) the meridional contrast of oceanic EKE with a 4–12-month lag after 1994. Some of these features are now investigated in more detail.

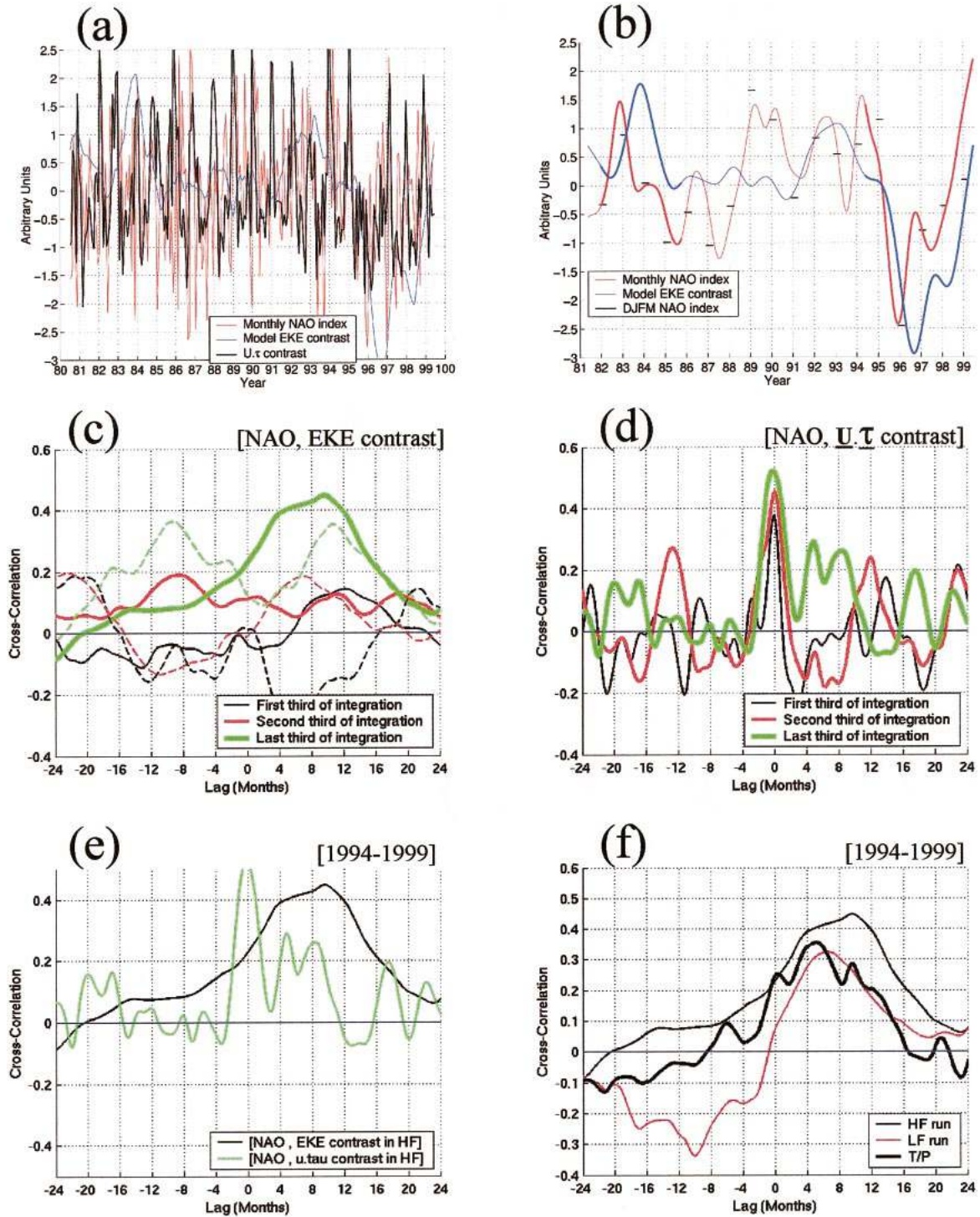


FIG. 5. (a) Normalized anomalies (with respect to the whole time series) of the following quantities in the HF simulation: monthly NAO index (red; Hurrell 1995), meridional contrast of EKE (blue) and of the energy input by the wind, i.e.,  $(\mathbf{u} \cdot \boldsymbol{\tau})_{\text{North}} - (\mathbf{u} \cdot \boldsymbol{\tau})_{\text{South}}$ , where  $\mathbf{u}$  and  $\boldsymbol{\tau}$  are the monthly surface model velocity and wind stress, respectively. (b) Blue and red lines from (a) after low-pass filtering. The 1994–99 period from which (c), (d), (e), and (f) were built is highlighted by thick lines. The 1982–85 period is also highlighted. (c) Cross correlations  $C(t)$  between the monthly NAO index and the EKE contrast over the three thirds of the period of 1980–99 in the HF simulation. Plain and dashed lines correspond to HF and PF runs, respectively. In every panel, NAO index leads at positive lags. (d) Cross correlation between the NAO index and the meridional contrast of the energy input by the wind during the three thirds of the HF integration. (e) Cross correlation between the NAO index and the EKE contrast (black line) and between the NAO index and the meridional contrast of the energy input by the wind in the HF run over the period of 1994–99 [green corresponds to the latest thick lines in (a) and (b)]. (f) Cross correlation between the NAO index and the EKE contrast diagnosed from the HF run (thin black line), from the LF run (red line), and from T/P data (thick black line) over the period of 1994–99.

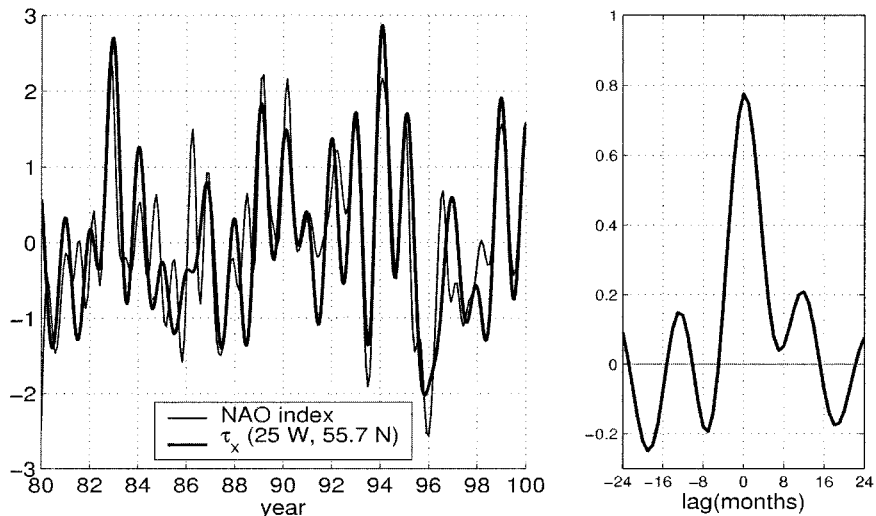


FIG. 6. (left) Evolution of the normalized NAO index thin line and the normalized anomaly of the zonal wind stress at 55.7°N, 25°W throughout the HF integration thick line. The NAO index is taken from Hurrell (1995). (right) Lagged correlation between the NAO index and the wind stress at the same location.

*c. Apparent absence of the link between NAO and EKE contrast before 1994*

This NAO–EKE link is not always clearly present in the model results. There are two possible explanations. First, it is possible that NAO-related, interannual atmospheric fluctuations may need to exceed a threshold to trigger changes in EKE contrast or make this response noticeable. This possibility is consistent with the fact that periods of possible NAO driving (i.e., 1994–99 and, perhaps, 1982–84) coincide with two major fluctuations of the NAO index. Second, and an alternative, the NAO–EKE link may always exist in the real world, but the forcing used in the HF simulation might be inaccurate in its NAO structure. Of these two, we prefer the first explanation, because the change in forcing (1 January 1994) did not affect the correlation found throughout the HF integration between the observed NAO index and the model wind forcing at important NAO locations (as shown in Fig. 6).

To summarize at this point, it appears that NAO-related atmospheric changes induce a quasi-immediate meridional redistribution of the energy provided by the wind to the ocean. Only strong NAO transitions are likely to trigger (or make emerge from other signals) meridional redistributions of surface EKE with a 4–12-month lag.

*d. Role of the westerlies and of the GS–NAC system on the fluctuations of the EKE contrast*

Figure 3 and SW99’s Fig. 1c highlight the gyre-scale extension of the relative change in surface EKE between 1993 and 1996. Absolute changes in EKE are, however, confined along the GS–NAC system. This suggests that

the modulations of the EKE meridional contrast mostly reflect the difference in eddy activity along the southwestern and northeastern parts of this current system. The EKE contrast is therefore likely to be controlled by the adjustment of the GS–NAC system, itself responding to the NAO cycle. This view is supported by two other facts.

The magnitude of the lag (4–12 months) found between the NAO index and  $EKE_{HF}$  contrast supports the proposed scenario. If the direct, local forcing of oceanic eddies by atmospheric fluctuations in the storm track was dominant, NAO index fluctuations would induce an oceanic response with essentially zero lag in terms of EKE contrast. The most plausible scenario is thus the following: the GS–NAC system adjusts to the slow displacement of the westerlies; this adjustment affects the distribution of baroclinic instability and EKE along the current and also the EKE meridional contrast.

Fluctuations of the NAO index correspond to simultaneous meridional migrations of the westerlies and of the associated storm track. High-frequency wind fluctuations such as those present in the storm track may contribute to force part of the oceanic EKE (Müller and Frankignoul 1981) although baroclinic instability is known to dominate throughout the ocean (Stammer 1998). Both latter features may thus contribute (through distinct mechanisms) to the EKE contrast evolution. The thick dashed line in Fig. 4d shows that between 1993 and 1999 the LF forcing, devoid of high-frequency atmospheric fluctuations, generates an evolution of the EKE contrast comparable to that derived from T/P (mutual correlation of 0.56) and that from the HF simulation. Although values of  $C(\text{lag})$  might be marginally significant in the LF simulation,  $EKE_{LF}$  contrast lags the NAO

by 4–8 months (Fig. 5f), consistent with  $EKE_{HF}$  and  $EKE_{TP}$  contrasts. The main features of the model response to NAO in terms of EKE contrast are thus induced by the nonsynoptic, slow evolution of the atmosphere. EKE contrast fluctuations probably follow the adjustment of the GS–NAC system to the NAO cycle through modifications of baroclinic instability (the main EKE source in this current). Nevertheless, the model–data agreement in terms of EKE contrast is better at time scales shorter than about 1 yr in the HF simulation than in the LF simulation (Fig. 4d), showing that high-frequency wind fluctuations contribute to the observed EKE contrast.

Richardson (1983) reported a comparable 4-month lag between the wind eddy energy at synoptic time scales and the oceanic EKE derived from surface drifters in the NAC (within a box centered along 47°N). This observation may explain the higher cross correlations around 4 months in the HF run as compared with LF. Figure 5f also shows that the synoptic part of the HF forcing is responsible for the presence of an NAO-forced response at longer lags (6–12 months) in terms of EKE contrast. This feature might involve nonlinear dynamics, and further investigation is required to explain it.

#### *e. On the processes at work*

The 4–12-month lag found between NAO and EKE contrast probably involves at least two time scales. One is required for the ocean to adjust to wind changes, and the other is likely to match the growth rate of mesoscale eddies. This latter time scale should not exceed a few weeks, according to the linear baroclinic instability analyses done by Beckmann (1988) and Beckmann et al. (1994). The oceanic adjustment to changes in the wind forcing thus probably involves time scales of several months, which is intermediate between the fast barotropic and slow baroclinic linear adjustment time scales of the basin (respectively on the order of days and years).

White and Heywood (1995) have noticed that, in accordance with the Sverdrup balance, the EKE veins associated with the NAC branches migrate in accordance with the line of zero wind stress curl on timescales shorter than 1 yr. This simple Sverdrupian argument apparently explains the sign relationship we found between the NAO index and the EKE meridional contrast. Also based on simple Sverdrupian arguments, Bersch et al. (1999) suggest that the weak westerlies observed during negative NAO situations induce a shrinking of the subpolar gyre. The time scale of this oceanic response is not particularly discussed in this latter study but is again shorter than 1 yr, as seen from the rapid evolution of the eastern North Atlantic stratification along a Greenland–Ireland section. This observed, rapid poleward shift of the NAC in low NAO situations is confirmed by numerical simulations (Eden and Wille-

brand 2001). These qualitative Sverdrupian arguments are thus consistent with our results.

Contours in Fig. 7 show the NAO-induced barotropic circulation anomaly as diagnosed from our HF run. This estimate should be considered as qualitative and informative, because 20-yr integration is formally too short to derive a statistically significant circulation anomaly. Figure 7 shows our counterpart of Marshall et al. (2001)’s Sverdrup-based “intergyre gyre,” in which primitive equations, realistic stratification, mesoscale turbulence, mechanical and buoyancy forcing, and topography are taken into account. It resembles Marshall et al.’s intergyre gyre but is elongated along the NAC path; it is also shifted southward and is flanked by a subpolar cyclonic anomaly influenced by topography. West of about 55°W, the eastward transport anomaly is located slightly north of the GS extension, meaning that the GS is stronger and located farther north in NAO+ phases [in accordance with Kelly (1991) and Frankignoul et al. (2001)]. East of about 50°W, the zero BSF anomaly contour follows the NAC path, suggesting that the main axis of the modeled NAC does not significantly shift meridionally during NAO+ phases. In agreement with Curry and McCartney (2001) and Flatau et al. (2003), the intensity of the NAC system and associated vertical shear increase during NAO+ phases: when compared with its 20-yr average, the NAC in 1989–95 is 5.5–6 Sv ( $1 \text{ Sv} \equiv 10^6 \text{ m}^3 \text{ s}^{-1}$ ) stronger across 40°W (3 Sv across 30°W). Such changes in baroclinic shear may locally explain EKE fluctuations through modulation of baroclinic instability. However, transport anomalies shown in Fig. 7 are not confined within one particular box but occur in both, without any preferred direction, and eventually (east of 30°W) split equally toward the subpolar and subtropical gyres. Fluctuations of the EKE contrast thus cannot be straightforwardly explained by NAO-forced circulation anomalies.

Complex (indirect, remote, nonlinear) adjustment processes might be involved in this adjustment. The ocean reacts to local and remote changes in atmospheric forcing, through the spatial and temporal integration of persistent forcing anomalies (Häkkinen 2001; Frankignoul et al. 2001; Visbeck et al. 2003). Rossby wave adjustment is certainly involved in these integrating processes. However, the real ocean dynamics (and those simulated by the present model) are more nonlinear and turbulent than assumed in most studies about oceanic adjustment, which are based on linear hypotheses or coarse- (about 1°) resolution model results. From idealized, eddy-resolving quasigeostrophic simulations, Dewar (2003) describes nonlinear modes involved in the adjustment of a turbulent ocean to NAO-like wind fluctuations. The most rapid mode corresponds to a barotropic-like adjustment process of the separated jet that starts just after the wind perturbation is applied. The nonlinear advective mechanism then needs an interval of a few months to complete the adjustment of the jet through a redistribution of the wind-forced potential

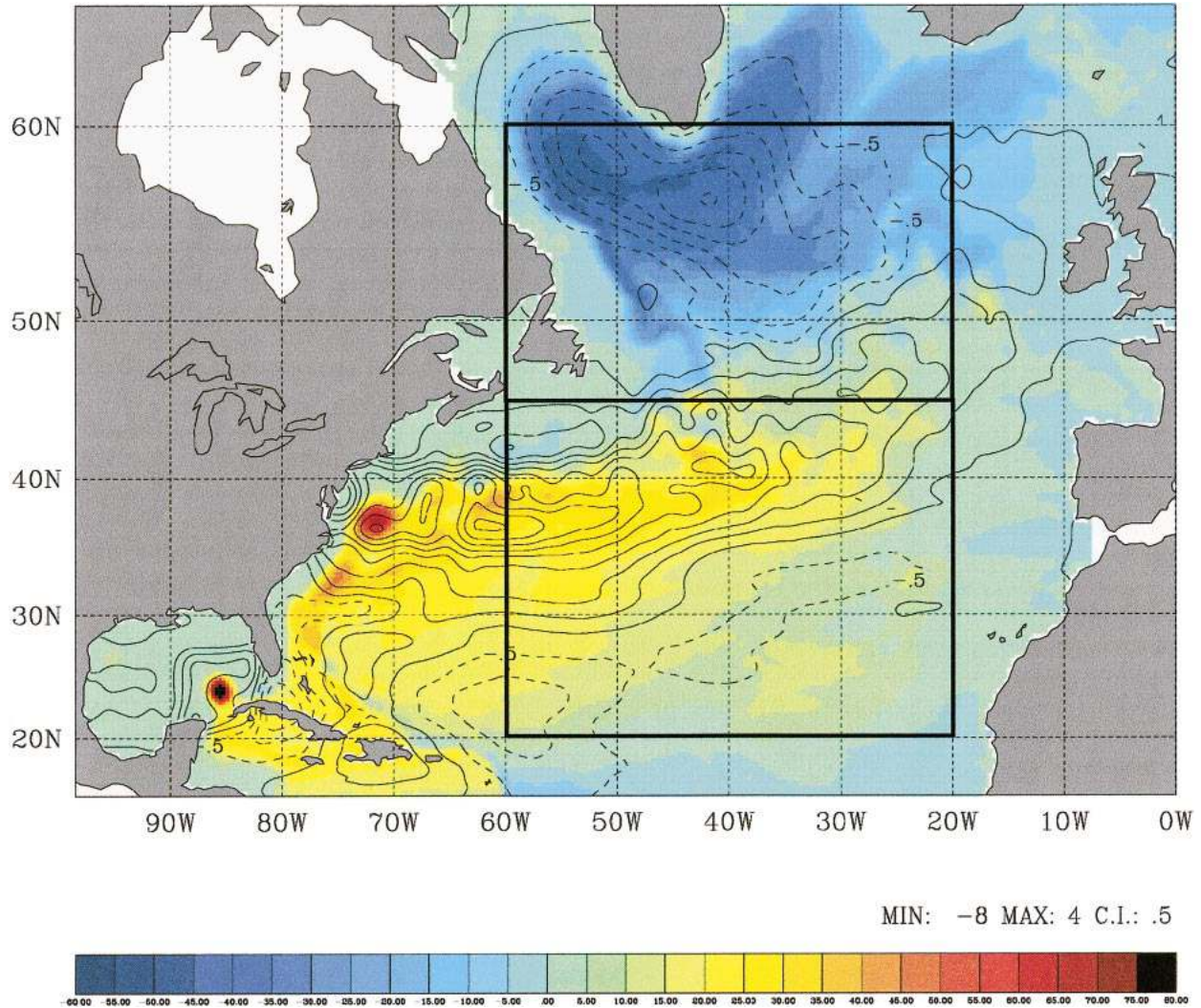


FIG. 7. Colors show barotropic streamfunction (BSF) from the HF simulation averaged between 1980 and 1999; color interval is 5 Sv. Contours show spatially smoothed BSF anomaly representative of NAO+ situations computed as the 1989–95 mean BSF minus the 1980–99 mean BSF; contour interval is 0.5 Sv, and plain (dashed) lines denote anticyclonic (cyclonic) anomaly. Our northern and southern boxes are superimposed.

vorticity (PV) anomaly. If the velocity is on the order of  $0.2 \text{ m s}^{-1}$  within  $O(1000 \text{ km})$ -wide western boundary recirculation cells, the jet should need about 2 months to adjust to the modified PV field. The ocean simulated in CLIPPER and in the real world is turbulent and quasi-geostrophic at first order but is influenced by many other factors (unlike this idealized western boundary current regime). The actual, realistic geometry might not influence the estimated time scale for two reasons. First, recirculation cells do exist in the real ocean, and, second, the suggested adjustment mechanism is regional (not wavelike), and thus its time scale does not depend on the domain extension. The 4–12 months of lag we found is somewhat longer than the 2 months estimated above, but we might need a few of these adjustment cycles for changes in the general circulation (and sub-

sequent EKE) to develop downstream of the western boundary.

## 6. Conclusions

Seven years of T/P data have been processed in the North Atlantic to investigate the interannual variability of EKE and, in particular, the behavior of a dipolar pattern previously mentioned by SW99. As showed by these authors, the subpolar (subtropical) EKE field was significantly stronger (weaker) than usual in 1993, and this contrast changed signs in 1996. We computed a simple EKE contrast index every 10 days from T/P data. The evolution of this index showed that the 1993 and 1996 situations described by SW99 were part of a more general, interannual fluctuation of the North Atlantic

eddy field. The same index was computed from the outputs of the  $1^\circ$  CLIPPER numerical simulation: the model realistically reproduces the evolution of the meridional EKE contrast during the T/P mission.

The observed and simulated EKE contrast indices were shown to follow the evolution of the NAO index with a 4–12-month lag over the T/P period. This link is not visible before 1994 in the simulation, suggesting that only strong NAO changes (such as those observed after 1993) can trigger such EKE meridional redistributions. Using two other model simulations, we showed that the 1993–99 slow EKE evolution 1) was significant—that is, it exceeded the intrinsic interannual variability of EKE obtained with a repeated seasonal cycle—and 2) was forced by the slow migration of the westerlies associated with the NAO cycle, with little influence from high-frequency atmospheric fluctuations.

The value of the lag itself suggests that the NAO-related atmospheric fluctuations first induce an adjustment of the NAC system, which then affects the meridional contrast of EKE. The time scale of the adjustment is slower (faster) than that of a linear barotropic (baroclinic) adjustment process. It is likely that local and basin-scale impacts of the atmospheric NAO cycle are integrated in time and space by the ocean on interannual time scales to produce this adjustment of EKE. Linear arguments [such as those developed by Eden and Willebrand (2001), or Sverdrup-based ideas] may explain the lag we diagnosed, but the nonlinear adjustment process studied by Dewar (2003) might have a contribution as well. In this scenario, NAO-related, wind-forced potential vorticity anomalies are advected in the inertial recirculations and affect the large-scale circulation within a few months.

Stammer et al. (2003, manuscript submitted to *J. Phys. Oceanogr.*) have shown that the variability of the eddy activity and distribution significantly affects the ocean general circulation at climatic time scales. Process-oriented investigations are necessary to answer the questions raised by the present study and to identify the processes involved in this NAO–EKE link.

*Acknowledgments.* This research was supported by the Climate Institute, a Center of Excellence sponsored by the Florida State University Research Foundation, and by the Centre National de la Recherche Scientifique (CNRS). Support for computations was provided by the Institut du Développement et des Ressources en Informatique Scientifique (IDRIS). The CLIPPER project was supported by the Institut National des Sciences de l’Univers (INSU), the Institut Français de Recherche pour l’Exploitation de la Mer (IFREMER), the Service Hydrographique et Océanographique de la Marine (SHOM), and the Centre National d’Etudes Spatiales (CNES). The altimeter products were produced by the CLS Space Oceanography Division as part of the Environment and Climate EC AGORA (ENV4-CT9560113) and DUACS (ENV4-CT96-0357) projects.

Author TP thanks Anne-Marie Tréguier, Alain Colin de Verdière, Nick Hall, Jorge Zavala, and Steve Morey for interesting discussions. Jean-Marc Molines is gratefully thanked for his contribution in the CLIPPER numerical simulations. Two anonymous reviewers provided helpful comments for which we are most appreciative.

## REFERENCES

- Barnier, B., 1998: Forcing the ocean. *Modeling and Parameterization*, E. P. Chassignet and J. Verron, Eds., Kluwer Academic, 45–80.
- Beckmann, A., 1988: Vertical structures of midlatitude mesoscale instabilities. *J. Phys. Oceanogr.*, **18**, 1354–1371.
- , C. W. Böning, B. Brügge, and D. Stammer, 1994: On the generation and role of eddy variability in the central North Atlantic Ocean. *J. Geophys. Res.*, **99**, 20 381–20 391.
- Bersch, M., J. Meincke, and A. Sy, 1999: Interannual thermohaline changes in the northern North Atlantic 1991–1996. *Deep-Sea Res.*, **46**, 55–75.
- Blanke, B., and P. Delecluse, 1993: Variability of the tropical ocean simulated by a general circulation model with two different mixed-layer physics. *J. Phys. Oceanogr.*, **23**, 1363–1388.
- Crosnier, L., B. Barnier, and A.-M. Tréguier, 2001: Aliasing of inertial oscillations in the  $1^\circ$  Atlantic circulation CLIPPER model: Impact on the mean meridional heat transport. *Ocean Modell.*, **3**, 21–32.
- Curry, R. G., and M. S. McCartney, 2001: Ocean gyre circulation changes associated with the North Atlantic Oscillation. *J. Phys. Oceanogr.*, **31**, 3374–3400.
- de Miranda, A. P., B. Barnier, and W. K. Dewar, 1999a: Mode waters and subduction rates in a high-resolution South Atlantic simulation. *J. Mar. Res.*, **57**, 1–32.
- , —, and —, 1999b: On the dynamics of the Zapiola anticyclone. *J. Geophys. Res.*, **104**, 213–244.
- Dewar, W. K., 1998: Topography and barotropic transport control by bottom friction. *J. Mar. Res.*, **56**, 295–328.
- , 2003: Nonlinear midlatitude ocean adjustment. *J. Phys. Oceanogr.*, **33**, 1057–1082.
- Ducet, N., and P.-Y. Le Traon, 2001: A comparison of surface eddy kinetic energy and Reynolds stresses in the Gulf Stream and the Kuroshio Current systems from merged TOPEX/Poseidon and ERS-1/2 altimetric data. *J. Geophys. Res.*, **106**, 16 603–16 622.
- Eden, C., and J. Willebrand, 2001: Mechanism of interannual to decadal variability of the North Atlantic circulation. *J. Climate*, **14**, 2266–2280.
- Flatau, M. K., L. Talley, and P. P. Niiler, 2003: The North Atlantic Oscillation, surface current velocities, and SST changes in the subpolar North Atlantic. *J. Climate*, **16**, 2355–2369.
- Frankignoul, C., G. De Coetlogon, T. Joyce, and S. Dong, 2001: Gulf Stream variability and ocean–atmosphere interactions. *J. Phys. Oceanogr.*, **31**, 3516–3529.
- Garnier, E., J. Verron, and B. Barnier, 2002: Variability of the South Atlantic upper ocean circulation: A data assimilation experiment with 5 years of TOPEX/Poseidon altimeter observations. *Int. J. Remote Sens.*, **24**, 911–934.
- Garnier, V., and R. Schopp, 1999: Wind influence on the mesoscale activity along the Gulf Stream and the North Atlantic Current. *J. Geophys. Res.*, **104** (C8), 18 087–18 110.
- Häkkinen, S., 2001: Variability in sea surface height: A qualitative measure for the meridional overturning in the North Atlantic. *J. Geophys. Res.*, **106**, 13 837–13 848.
- Hurrell, J. W., 1995: Decadal trends in the North Atlantic Oscillation regional temperatures and precipitation. *Science*, **269**, 676–679.
- Kelly, K. A., 1991: The meandering Gulf Stream as seen by the Geosat altimeter: Surface transport, position and velocity variance from  $73^\circ$  to  $46^\circ$  W. *J. Geophys. Res.*, **96**, 16 721–16 738.
- Klein, B., and G. Siedler, 1989: On the origin of the Azores Current. *J. Geophys. Res.*, **94**, 6159–6168.

- Legg, S., J. C. McWilliams, and J. Gao, 1998: Localization of deep ocean convection by a geostrophic eddy. *J. Phys. Oceanogr.*, **28**, 944–970.
- Le Traon, P. Y., F. Nadal, and N. Ducet, 1998: An improved mapping method of multisatellite altimeter data. *J. Atmos. Oceanic Technol.*, **15**, 522–534.
- Madec, G., P. Delecluse, M. Imbard, and C. Lévy, 1998: OPA 8.1 Ocean General Circulation Model reference manual. Institut Pierre-Simon Laplace Note du Pôle de Modélisation 11, 91 pp.
- Marshall, J., H. Johnson, and J. Goodman, 2001: A study of the interaction of the North Atlantic Oscillation with the ocean circulation. *J. Climate*, **14**, 1399–1421.
- Mueller, T. J., and G. Siedler, 1992: Multi-year current time series in the eastern North Atlantic Ocean. *J. Mar. Res.*, **50**, 63–98.
- Müller, P., and C. Frankignoul, 1981: Direct atmospheric forcing of geostrophic eddies. *J. Phys. Oceanogr.*, **11**, 287–308.
- Reynaud, T., P. Legrand, H. Mercier, and B. Barnier, 1998: A new analysis of hydrographic data in the Atlantic and its application to an inverse modelling study. *International WOCE Newsletter*, No. 32, WOCE International Project Office, Southampton, United Kingdom, 29–31.
- Reynolds, R. W., and T. M. Smith, 1995: A high resolution global sea surface temperature climatology. *J. Climate*, **8**, 1571–1583.
- Rhines, P. B., and W. R. Young, 1982: Homogenization of potential vorticity in planetary gyres. *J. Fluid Mech.*, **122**, 347–367.
- Richardson, P. L., 1983: Eddy kinetic energy in the North Atlantic from surface drifters. *J. Geophys. Res.*, **88**, 4355–4367.
- Rogers, J. C., 1990: Patterns of low-frequency monthly sea-level pressure variability (1899–1986) and associated wave cyclone frequencies. *J. Climate*, **3**, 1364–1379.
- Smith, W. H. F., and D. T. Sandwell, 1997: Global seafloor topography from satellite altimetry and ship depth soundings. *Science*, **277**, 1957–1962.
- Stammer, D., 1998: On eddy characteristics, eddy transports, and mean flow properties. *J. Phys. Oceanogr.*, **28**, 727–739.
- , and C. Wunsch, 1999: Temporal changes in eddy energy of the oceans. *Deep-Sea Res.*, **46**, 77–108.
- Sy, A., V. Schauer, and J. Meinke, 1992: The North Atlantic Current and its associated hydrographic structure above and eastwards of the Mid-Atlantic Ridge. *Deep-Sea Res.*, **39**, 825–853.
- Tréguier, A. M., and Coauthors, 1999: The CLIPPER project: High resolution modeling of the Atlantic. *International WOCE Newsletter*, No. 36, WOCE International Project Office, Southampton, United Kingdom, 3–5.
- , and Coauthors, 2001: An eddy permitting model of the Atlantic circulation: Evaluating open boundary conditions. *J. Geophys. Res.*, **106**, 22 115–22 129.
- , O. Boebel, B. Barnier, and G. Madec, 2002: Agulhas eddy fluxes in a  $1^\circ$  Atlantic model. *Deep-Sea Res.*, **50B**, 251–280.
- Visbeck, M., E. Chassignet, R. Curry, T. Delworth, B. Dickson, and G. Krahnmann, 2003: The ocean's response to North Atlantic Oscillation variability. *The North Atlantic Oscillation, Geophys. Monogr.*, No. 134, Amer. Geophys. Union, 113–146.
- White, M. A., and K. J. Heywood, 1995: Seasonal and interannual changes in the North Atlantic subpolar gyre from *Geosat* and *TOPEX/Poseidon* altimetry. *J. Geophys. Res.*, **100**, 24 931–24 941.